Available online at www.sciencedirect.com
SCIENCE DIRECT®
Physica D 192 (2004) 138–160
PHYSICA D
www.elsevier.com/locate/physd

Chaotic firing in the sinusoidally forced leaky integrate-and-fire model with threshold fatigue

Maurice J. Chacron [a,*], André Longtin [a], Khashayar Pakdaman [b]

[a] *Department of Physics, University of Ottawa, 150 Louis Pasteur, Ottawa, Canada K1N 6N5*
[b] *Inserm U444, 27 Rue Chaligny, 75571 Paris Cedex 21, France*

Received 26 March 2003; received in revised form 13 December 2003; accepted 29 December 2003
Communicated by J.P. Keener

Abstract

The leaky integrate-and-fire (LIF) model is one of the elementary neuronal models that has been widely used to gain understanding of the behavior of many excitable systems. The sinusoidally forced standard leaky integrate-and-fire model reproduces the quasiperiodic and phase locked discharge trains observed experimentally in neurons. However, this basic model fails to generate chaotic firing, whereas this form of behavior has been observed experimentally. We modify the standard LIF through the introduction of threshold fatigue responsible for progressive decrease of excitability during high frequency firing, as observed experimentally. We show that the dynamics of this neuron model under sinusoidal forcing are governed by the iterates of an annulus map and derive expressions for its two characteristic Lyapunov exponents. Using these exponents, it is shown that chaotic dynamics are possible for this model, unlike the standard leaky integrate-and-fire model. Chaotic dynamics occur when memory effects are strong and only under certain forms of threshold fatigue.

PACS: 05.40.−a; 87.22.Jb; 87.19.La; 87.19.Bb; 87.17.Nn

Keywords: Non-linear dynamics; Chaos; Lyapunov exponents; Integrate-and-fire dynamical systems; Neuron

1. Introduction

Discontinuous dynamical systems are playing an important role in the study of many physical (see e.g. [25]) and biological systems (e.g. neurons, [34]). There have been recent advances on techniques for analyzing such systems [21]. Our work examines the dynamics of one such system of relevance to the behavior of excitable systems such as neurons.

Neurons transform incoming information into trains of action potentials that are transmitted to and processed by other neurons. An action potential is an "all-or-none" stereotyped response to a stimulus. Typically the action potential has a much shorter time scale (order of milliseconds) than the other time scales in the neuron (over tens or hundreds of milliseconds). For this reason, it can be approximated as a delta function in neuronal models.

* Corresponding author. Tel.: +1-613-56258008258; fax: +1-613-5625434.
E-mail address: mchacron@physics.uottawa.ca (M.J. Chacron).

0167-2789/$ – see front matter © 2004 Elsevier B.V. All rights reserved.
doi:10.1016/j.physd.2003.12.009

One example where this approximation has been widely used is the leaky integrate-and-fire (LIF) model, arguably the most elementary spiking neuron model [34]. In this model, the membrane voltage is discontinuously reset to a fixed value once it reaches a certain threshold. Despite its simplicity, this model is able to reproduce a great deal of known features of real neurons including the all-or-none response and the postdischarge refractoriness. It also reproduces rectification and phase locking behavior of neurons under sinusoidal forcing [3,30,33]. However, it fails to reproduce some key features observed experimentally in certain neurons like adaptation [9] and chaotic behavior under sinusoidal stimulation [10,19,26].

Analyzing the response of neurons to controlled stimuli has been one of the methods used to determine the relationship between incoming stimuli and the response they elicit in neurons. Historically, among the various signals that have been used for this purpose, sinusoidal stimuli have played a prominent role. Such stimuli were first used as a means to estimate the transfer function of preparations such as stretch receptors, considered as linear black boxes (see e.g. [29]). The same class of stimulation also proved the limitation of the linear approach by revealing that periodically forced receptors could display substantial non-linearities in the form of rectification and phase locking [12]. Similar non-linear responses were observed in diverse preparations (e.g. [36]), eventually opening the door for the analysis of neuronal behavior from the standpoint of non-linear dynamical systems theory. This in turn was instrumental in unraveling that the variability in discharge times of sinusoidally forced neurons was not necessarily due to noise, but could as well be due to chaotic behavior [1,16].

Since these early studies, one direction of investigation has been to determine the basic neuronal properties that can underlie the various behaviors observed experimentally. One approach to this problem has been to construct minimal models that present only the basic biologically plausible properties necessary to reproduce a given class of responses. This approach can be instrumental in determining the contribution of different neuronal properties in neuronal coding. For instance, the sinusoidally forced standard perfect integrate-and-fire model, one of the simplest neuronal models, reproduces rectification, but not phase locking [19,20,33]. However, by augmenting this elementary model with a leak current, one obtains the standard leaky integrate-and-fire model that reproduces both rectification and phase locking [3,30,33] to the input. In this way, the systematic analysis and comparison of these elementary models, confirmed that, not surprisingly, the firing threshold was responsible for rectification, and revealed as well that forgetful integration due to the leak current was instrumental for obtaining phase lockings. However, the standard LIF fails to reproduce more complex dynamics such as chaotic ones. The concern of the present study is the construction of a minimal model capable of generating chaos by augmenting the standard LIF.

In this paper, we provide a non-linear dynamical analysis of a modified LIF model incorporating threshold fatigue under sinusoidal forcing. This particular modification is biologically motivated [4] and has been previously used with great success to model different classes of neurons [7–9,13,17,18,23,24,27,28,32,35] that display adaptation. It has furthermore been shown that threshold fatigue could model very different physiological mechanisms including an ionic current giving rise to adaptation [23], synaptic depression [15], and recurrent inhibition [11].

The paper is organized as follows. We first present the model in Section 2. After showing that it is equivalent to an annulus map, we derive expressions for its Lyapunov exponents by generalizing Coombes's method [10] to evaluate Lyapunov exponents for the standard LIF in Section 3. Numerical simulations in Section 4 demonstrate that chaotic dynamics are possible. It is known that successive discharge phases of the standard LIF model under sinusoidal (or more generalized periodic) forcing are given by iterates of a monotonically increasing circle map [19,26,30] (we refer to a circle map as monotonically increasing when any lift associated to it is monotonically increasing, and henceforth cannot give rise to chaotic dynamics. However, no such restrictions exist for the annulus map which can thus display chaotic dynamics. We further reduce our model to a circle map in Section 5 which we show to be non-monotonic for certain parameters in Section 6 and thus can also display chaotic dynamics.

2. The model

We consider a sinusoidally forced LIF with dynamic threshold given by the following differential equations and firing rules:

$$\frac{dv}{dt} = -\frac{v}{\tau_v} + \mu + a\,\sin(wt) \quad \text{if} \quad v(t) < s(t), \tag{1}$$

$$\frac{ds}{dt} = \frac{s_r - s}{\tau_s} \quad \text{if} \quad v(t) < s(t), \tag{2}$$

$$v(t^+) = v_0 \quad \text{if} \quad v(t) = s(t), \tag{3}$$

$$s(t^+) = s_0 + W[s(t), \alpha] \quad \text{if} \quad v(t) = s(t), \tag{4}$$

where v is the voltage, s is the threshold, μ is a constant input stimulation, a and w are the respective amplitude and angular frequency of the sinusoidal forcing, τ_v and τ_s are the time constants for voltage and threshold, respectively, and s_r is the value at which the threshold would stabilize in the absence of firing. Firing occurs when the voltage reaches the threshold. Following this, the voltage is reset to v_0 (Eq. (3)) and the threshold is set to $s(t^+) = s_0 + W[s(t), \alpha]$, where s_0 is a parameter and W is a positive monotonically increasing function of s and α with $W(s, 0) = 0$. The parameter α controls the amount of memory in the system. The particular function W used in model studies can be linear or non-linear as its exact shape is not currently known experimentally and will likely depend on the specifics of the neuron under study. Typical functions W are $W(s, \alpha) = \alpha(s - s_r)$ and $W(s, \alpha) = \exp[\alpha(s - s_r)] - 1$ and we will study the impact of the functional form for W on the model's dynamics. When $\alpha = 0$, the threshold is always reset to the value s_0. The model thus displays no memory and no interspike interval correlations [9]. As we increase α, memory effects become more important as $W(s, \alpha)$ grows with respect to s_0. Most previous models used $\alpha = 1$ [7,8,13,23,24,27,28,35] and the effects of varying α on adaptation, ISI statistics, and firing behavior was explored in [9]. The time evolution of the dynamics are graphically illustrated in Fig. 1.

We denote by $v(t, t_n)$ and $s(t, t_n, S_n^+ \equiv s(t_n^+))$ the voltage and threshold solutions at time t comprised between the nth and $n + 1$th discharge times ($t_n < t < t_{n+1}$) and assume, without loss of generality, that $v_0 = 0$. Furthermore,

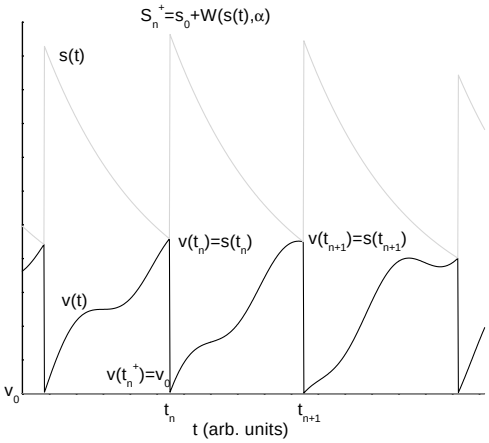

Fig. 1. The dynamics of the voltage $v(t)$ (black line) and the threshold $s(t)$ (grey line) in the model given in Eqs. (1)–(4). An action potential occurs when $v(t) = s(t)$. Immediately after, $v(t^+) = v_0$ while $s(t^+) = s_0 + W(s(t), \alpha)$.

we assume that $\mu\tau_v > 0$ and $s_r > 0$. Given the initial conditions $v(t_n, t_n) = 0$ and $s(t_n, t_n, S_n^+) = S_n^+$, $t \geq t_n$, and provided that no firing occurs on the interval $[t_n, t]$, these solutions are given by

$$v(t, t_n) = \mu\tau_v \left(1 - \exp\left[\frac{t_n - t}{\tau_v}\right]\right) + \frac{a\tau_v}{1 + w^2\tau_v^2}[\sin(wt) - w\tau_v \cos(wt)] - \frac{a\tau_v \exp[(t_n - t)/\tau_v]}{1 + w^2\tau_v^2}[\sin(wt_n) - w\tau_v \cos(wt_n)], \tag{5}$$

$$s(t, t_n, S_n^+) = s_r + (S_n^+ - s_r)\exp\left(\frac{t_n - t}{\tau_s}\right). \tag{6}$$

The model generates sustained firing if the sequence $\{t_n\}$ of discharge times is unbounded, i.e. $t_n \to \infty$. A necessary and sufficient condition for sustained firing is given by

$$\mu\tau_v + \frac{a\tau_v}{\sqrt{1 + w^2\tau_v^2}} > s_r. \tag{7}$$

This condition has already been proven to be necessary and sufficient in the periodically forced standard LIF [26]. We now prove that this condition is necessary and sufficient for sustained firing in the LIF with threshold fatigue. Condition (7) is obviously sufficient for sustained firing in the LIF with threshold fatigue. In order to establish that it is also necessary, we need to prove that when it fails, then the LIF with threshold fatigue generates at most a finite number of discharges. To see this, we remark that the threshold of the LIF with fatigue satisfies $s \geq s_r$ at all times, and regardless of the firing history. Hence, if an input produces at most a finite number of firing in the standard LIF with constant threshold fixed at s_r, it does necessarily so in the LIF with threshold fatigue. Given that when condition (7) fails, the standard LIF with constant threshold fixed at s_r fires at most a finite number of times, the same must hold for the LIF with threshold fatigue.

Remarkably, this condition does not depend on the initial condition: there are no parameter sets such that for some initial conditions the firing stops in a finite time while for others it would persist indefinitely. We will assume that the condition for sustained firing holds throughout the paper.

The continuous-time LIF dynamics are not smooth due to the reset condition, and so the standard theory of dynamical systems does not apply directly to this model. However, this problem can be overcome by noticing that the LIF dynamics are in fact equivalent to the iterates of a map of successive firing times, that is to a discrete-time dynamical system. This formulation can then be used to analyze the dynamics of the LIF. More precisely, the model described in Eqs. (1)–(4) is equivalent to a two-dimensional annulus map [9]. Given the nth discharge time t_n and the corresponding postdischarge threshold S_n^+, the $n + 1$th firing time t_{n+1} is given by

$$t_{n+1} = H_1(t_n, S_n^+) \stackrel{\text{def}}{=} \inf\{t : t > t_n, v(t, t_n) = s(t, t_n, S_n^+)\}, \tag{8}$$

and the corresponding postdischarge threshold $s(t_{n+1}^+, t_n, S_n^+) \equiv S_{n+1}^+$ is given by

$$S_{n+1}^+ = H_2(t_n, S_n^+) \stackrel{\text{def}}{=} s_0 + W(s(t_{n+1}, t_n, S_n^+), \alpha). \tag{9}$$

A two-dimensional map H can be defined as: $H : (t_n, S_n^+) \to (t_{n+1} = H_1(t_n, S_n^+), S_{n+1}^+ = H_2(t_n, S_n^+))$ on $[0, \infty) \times [s_0 + W(s_r, \alpha), s_0 + W(V_{\text{upper}}, \alpha)]$, where $V_{\text{upper}} = \mu\tau_v + 2a\tau_v/\sqrt{1 + w^2\tau_v^2}$ is an upper bound to the maximum value of the voltage $V_{\max} = \mu\tau_v + a\tau_v/\sqrt{1 + w^2\tau_v^2}$.

It is convenient to introduce the firing phase as in [10] as

$$\phi_n = 2\pi\left\{\frac{t_n}{T} - \text{int}\left[\frac{t_n}{T}\right]\right\}, \tag{10}$$

where the int[·] denotes the integer part and $T \equiv 1/f = 2\pi/\omega$ is the forcing period.

Given that $H_1(t+T,S) = T + H_1(t,S)$ and $H_2(t+T,S) = H_2(t,S)$ for all t and S, the map H is a lift of the annulus map $\tilde{H} = (\tilde{H}_1, \tilde{H}_2)$ on $[0, 2\pi) \times [s_0 + W(s_r, \alpha), s_0 + W(V_{\text{upper}}, \alpha)]$:

$$\tilde{H}_1(\phi_n, S_n^+) = \frac{2\pi}{T} H_1\left(\frac{T}{2\pi}\phi_n, S_n^+\right) \text{ modulo } T, \tag{11}$$

$$\tilde{H}_2(\phi_n, S_n^+) = H_2\left(\frac{T}{2\pi}\phi_n, S_n^+\right). \tag{12}$$

For the standard LIF (i.e. when $\alpha = 0$), the threshold remains constant throughout time, so that $\tilde{H}_2$ is constant, and we retrieve the one-dimensional map $\tilde{H}_1$ that has been used in previous studies of periodically forced LIFs [19,26,30].

3. Lyapunov exponents of the model

The main purpose of our study is to establish that the modified LIF can exhibit chaotic dynamics. This is done by establishing that there are regimes in which the model displays sensitive dependence on initial conditions as indicated by a positive Lyapunov exponent. To this end, we first derive the expression for the Lyapunov exponents of the model given in Eqs. (1)–(4). While both differential equations governing interdischarge dynamics of the voltage and the threshold are linear, the discontinuous jumps occurring at each discharge introduce non-linearity in the dynamics of this model. The main step in the derivation of the Lyapunov exponents consists therefore in evaluating the consequence of these discontinuities on solutions starting from nearby initial conditions.

For smooth continuous-time dynamical systems, Lyapunov exponents can be derived either directly from the variational equation associated with the continuous-time description of the dynamics or from the variational equation associated with the discrete-time description of the dynamics through iterates of a Poincaré map (see e.g. [31]). In the same way, there are two possible standpoints for the evaluation of the Lyapunov exponents of the non-smooth periodically forced LIF with threshold fatigue. One is to consider the exponents associated with the annulus map introduced in the previous section, and estimate the growth or decay rates of perturbations of the postdischarge threshold and phases. The other possibility is to estimate the growth and decay rates of perturbations of the postdischarge threshold and voltage that will of course depend on the evolution equations of these variables. The signs of the Lyapunov exponents do not depend on the method, even though their absolute values may. For our purpose, which is to determine the existence of chaos, either method is acceptable. We selected the second one because it proceeds similarly to previous studies of the standard LIF [10] using ideas developed for the study of impact oscillators [21,25]. The derivation and expressions for the Lyapunov exponents are presented in Appendix A.

4. Evidence for chaotic firing: numerical simulations

In many studies of periodically forced systems, the focus is on the occurrence of particular periodic dynamics such as phase locking regions, and their organization into Arnold tongues. An illustrative example for the standard LIF is provided by Keener et al. [19]. In our investigation of the dynamics of the sinusoidally forced LIF with fatigue, we also observed such regimes. However, here, we do not proceed with their description, as our main concern is not the organization of periodic orbits, but to show that the modified LIF is capable of producing chaos. Therefore, we limit the presentation of numerical results to examples of chaotic dynamics.

The numerical simulations of forced LIF model with threshold fatigue were performed as follows. Starting from $t_0 = 0$, the analytical solutions $v(t, 0)$ and $s(t, 0, S_0^+)$ with S_0^+ chosen arbitrarily were used to find the firing time $t_1 > 0$ that is the smallest solution of

$$v(t_1, t_0) = s(t_1, t_0, S_0^+). \tag{13}$$

The threshold value S_1^+ immediately after t_1 was computed as

$$S_1^+ = s_0 + \exp\{\alpha[s(t_1, t_0, S_0^+) - s_r]\} - 1. \tag{14}$$

The smallest solution t_2 of $v(t, t_1) = s(t, t_1, S_1^+)$ was then computed. Following this recursive procedure, we obtained the firing time and threshold sequences $\{t_i\}_{i=1}^N$ and $\{S_i^+\}_{i=1}^N$, respectively for N large. Typically, we took N to be greater than 1000. This allowed us to numerically estimate the Lyapunov exponents of the system following the procedure outlined in Appendix A.

We have previously explored the influence of the parameter α on ISI statistics and adaptation displayed by the model [9]. In order to explore the existence of fatigue-induced chaotic dynamics, we proceeded here with a systematic analysis of the influence of the parameter α and the function W on the asymptotic behavior of the model. Thus, we performed numerical simulations using different values of α and different functional forms for W starting from $\alpha = 0$ and incrementing between each simulation.

The observations based upon these systematic numerical investigations carried out for diverse parameter sets can be summarized as follows. For $\alpha = 0$, the leading Lyapunov exponent of the model is either negative or zero. It does not take on positive values. In fact, simulations suggest that without threshold fatigue, the model behaves in the same way as the standard LIF [19] that produces phase locked, quasiperiodic dynamics and strange non-chaotic behavior. Simulations at low values of α produce similar observations. As α is increased, there may be drastic qualitative changes in the asymptotic dynamics of the model, in the sense that the leading Lyapunov exponent becomes positive, while, simultaneously, the discharge phases become irregular and unpredictable. In such cases, simulations of solutions of nearby initial conditions confirm the sensitive dependence on initial conditions, since they grow rapidly apart with time. We argue that this numerical evidence supports the fact that these regimes correspond to chaos. These constitute the main numerical evidence for fatigue being capable of producing chaos in neuronal responses.

An illustrative example of the results is shown in Fig. 2, that represents the impact of increasing α on the dynamics of the system. Fig. 2a shows a bifurcation diagram obtained while varying the parameter α, while Fig. 2b shows the leading Lyapunov exponent of the system $\Gamma = \max(\lambda, \mu)$ for the same range of α. The parameter values are chosen such that for $\alpha = 0$, the model exhibits periodic phase locking dynamics. This regime alternates with quasiperiodic behavior as α is increased. This is similar to what is seen in the LIF model under sinusoidal forcing [10]. However, as α is increased further, chaotic dynamics start appearing as shown in Fig. 2. This illustrates the rich dynamical behavior exhibited by the model.

The lines in the bifurcation diagram correspond to periodic firing where the interspike intervals take on a finite number of values. The thick parts correspond to regimes where the interspike interval takes either a countable but very large number of values, or an uncountable value. Given that in the diagram there are only finitely many points represented, it is not possible to state whether these regimes correspond to periodic orbits with large periods, quasiperiodic or chaotic regimes. The leading Lyapunov exponent brings in valuable information in this respect, as the exponents associated with these regimes are respectively, negative, zero and positive. The ranges of positive exponents in Fig. 2b suggest that, as expected, there are indeed chaotic regimes within these regions. Besides the existence of chaos, Fig. 2 contains valuable information about the scenario leading to such dynamics as α is varied. The diagram reveals that tangent bifurcations (near $\alpha = 31$) and period doubling cascades can lead to chaotic

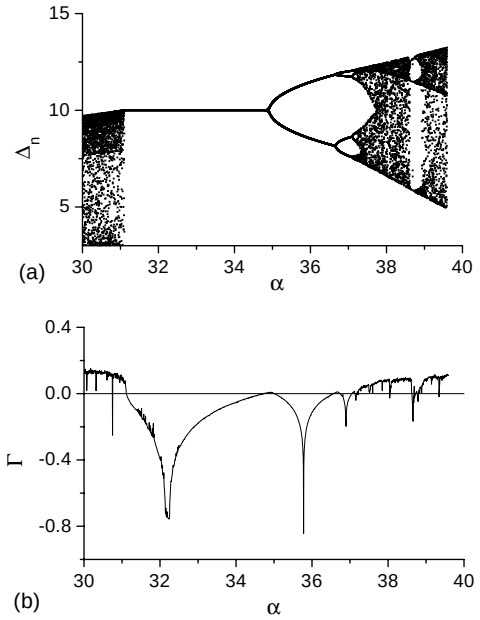

Fig. 2. (a) ISI Δ_n as a function of α illustrating the complex dynamics exhibited by our model. Period doubling bifurcations as well as tangent bifurcations are seen. (b) Largest Lyapunov exponent Γ of the model as a function of α. Γ is positive for certain values of α indicating sensitivity to initial conditions and thus chaotic dynamics. Parameter values were: $s_r = 0.0268$, $\tau_s = 0.8$, $\tau_v = 1$, $a = 0.1732$, $w = 0.62832$, $\mu = 0.25$, $s_0 = 0.1$. We further used $W(s, \alpha) = \exp[\alpha(s - s_r)] - 1$. We used 1800 time units worth of data to estimate the Lyapunov exponents for each value of α.

dynamics in the model. Our numerical explorations revealed the role of another factor, besides α, in the onset of chaos.

Sensory neurons adapt in different ways, some faster and more markedly than others. To account for this, we used different fatigue functions W to check how the shape of this function affected the possibility of the onset of chaos. The simulations showed that this factor could indeed be important in this respect. For instance, when W was taken as a linear function, the simulations did not produce chaotic dynamics (not shown), while when W increased exponentially, such regimes were readily observed (Fig. 2). However, a sigmoidal form of W did yield chaotic dynamics (not shown). At this point, the simulations do not suffice to rule out the possibility of chaos for the linear fatigue function, however, they do indicate that, if there are chaotic dynamics for this variant, then they occur in more restricted parameter ranges than for variants with rapidly increasing W.

In summary, our numerical investigations of the dynamics of the sinusoidally LIF with fatigue showed that this model, unlike the standard LIF, is capable of producing chaotic dynamics, provided that the fatigue function W increase sufficiently rapidly and that the fatigue parameter α be large enough. In the following section, we try to clarify the underlying mechanisms by analyzing a particular regime where the model dynamics can be further simplified.

5. Approximation with a circle map

To gain deeper understanding of the chaotic dynamics brought about by the parameter α, we reduce the dynamics to a one-dimensional map. In general, the reduction of the dimension from 2 to 1 is not possible. Such a scheme

is valid under special conditions, that require extra hypotheses on the parameters. Schematically, the reduction is possible when the voltage transient dynamics are substantially faster than the evolution of the threshold. In heuristic terms, this assumption means that, after each discharge, the voltage rapidly reaches its asymptotic oscillatory regime before crossing the threshold. In this way, we can neglect the transient voltage dynamics following each discharge. This allows us to focus on only one equation, that of the threshold decay. In this way, we are able to reduce the model to a single one-dimensional system whose dynamics are captured by a circle map.

5.1. Definition of the reduced model

We first introduce the reduced model's voltage and threshold as

$$\hat{v}(t) = V_r + A\ \sin(\Omega t - \phi), \tag{15}$$

$$\hat{s}(t, t_n, S_n^+) = s_r + (S_n^+ - s_r)\exp(t_n - t). \tag{16}$$

In fact Eq. (16) defining $\hat{s}$ is identical to Eq. (6) defining the threshold of the full model, so that from this point on we use the same notation s (without the "hat") for both models.

The successive discharge times and postdischarge thresholds of this model are defined similarly to those of the full model (Eqs. (8) and (9)) as

$$t_{n+1} = F_1(t_n, S_n^+) \stackrel{\text{def}}{=} \min\{t : t > t_n \ \text{ and } \ \hat{v}(t) = s(t, t_n, S_n^+)\}, \tag{17}$$

$$S_{n+1}^+ = F_2(t_n, S_n^+) \stackrel{\text{def}}{=} s_0 + W(s(t_{n+1}, t_n, S_n^+), \alpha). \tag{18}$$

At this stage, the description of the reduced model is through a two-dimensional map $F = (F_1, F_2)$. Similarly to the full model, this map is a lift of a map of the annulus that we denote by $\tilde{F}$. We show that the dynamics of the iterates of this map can be derived from those of a one-dimensional circle map. More precisely, the essential difference between the full and reduced models resides in that $\hat{v}$ (Eq. (15)), unlike v (Eq. (8)), does not depend explicitly on t_n. Taking advantage of this, and that $s(t_n, t_{n-1}, S_{n-1}^+) = \hat{v}(t_n)$, we can rewrite Eq. (18) at the $n-1$th iterate as

$$S_n^+ = F_2^{\text{red}}(t_n) \stackrel{\text{def}}{=} s_0 + W(\hat{v}(t_n), \alpha), \tag{19}$$

which can be substituted into Eq. (17) to yield a one-dimensional map $t_n \to t_{n+1}$:

$$t_{n+1} = f(t_n) \stackrel{\text{def}}{=} F_1(t_n, F_2^{\text{red}}(t_n)). \tag{20}$$

A necessary and sufficient condition for the existence of t_{n+1} is

$$V_r + A > s_r. \tag{21}$$

This is similar to condition (7) stating that the firing is sustained if and only if the maximal voltage is larger than the resting threshold. Provided this condition is satisfied, we have $f(t) + T = f(t + T)$ for $T = 2\pi/\Omega$, so that f is the lift associated to a degree-one circle map $\tilde{f}$ defined as $\theta \to \Omega f(\theta/\Omega)$ modulo 2π.

In terms of the dynamics on the annulus, the above result shows that (i) the subset of the annulus defined as $C = \{(\theta, S) : S = s_0 + W(\hat{v}(\theta/\Omega), \alpha)\}$ is forward invariant under $\tilde{F}$ (i.e. $\tilde{F}(C) \subset C$), (ii) the subset C is absorbing as for any (θ, S) in the annulus, we have $\tilde{F}(\theta, S) \in C$ and (iii) the dynamics of $\tilde{F}$ on C are given by the iterates of the circle map $\tilde{f}$. In other words, the reduced model defined on the annulus can indeed be reduced to a circle map. The map f is not necessarily onto, so that in the following we make the extra assumption:

$$V_r - s_r > A\sqrt{1 + \Omega^2}. \tag{22}$$

Condition (22) ensures that f is onto, and furthermore, that the voltage and threshold curves intersect transversally (cannot be tangent to one another) at any discharge time. This latter condition proves important when considering the full model as a perturbation of the reduced model. Finally, we also assume that $s_0 > V_r + A$, so that, even when adaptation α is set to zero, the reduced model is well defined: all postdischarge thresholds are above the voltage. This is made necessary because in the reduced model there is no postdischarge voltage reset.

5.2. Pointwise convergence of the full model to the reduced model

Theorem 1. *Let the maps H and F be defined as above. Let time be rescaled to the threshold time scale $t \to t/\tau_s$, and set $V_r = \mu\tau_v$, $A = a\tau_v/\sqrt{1+w^2\tau_v^2}$, $\Omega = w\tau_s$, $\cos(\phi) = 1/\sqrt{1+w^2\tau_v^2}$ with $\phi \in [0, \pi/2]$. As $\tau_v \to 0$, while holding V_r, A and ϕ constant, the map H of the full model converges pointwise to the map F of the reduced model defined above.*

Proof. We start with a preliminary remark concerning the interdischarge intervals of the full and reduced models. We rewrite the voltage of the full model as

$$v(t', t) = \hat{v}(t') + g(t', t, \tau_v), \tag{23}$$

where $\hat{v}$ is given in Eq. (15) and g is defined as

$$g(t', t, \tau_v) = \exp\left[-\frac{t'-t}{\tau_v}\right](A\,\sin(\Omega t - \phi) - V_r) \quad \text{if} \quad \tau_v > 0, \tag{24}$$

$$g(t', t, \tau_v) = 0 \quad \text{if} \quad \tau_v = 0. \tag{25}$$

From condition (22), we have that $A - V_r < A\sqrt{1+\Omega^2} - V_r < -s_r < 0$, so that, for $\tau_v > 0$, $g(t', t, \tau_v) < 0$ and $v(t', t) < \hat{v}(t')$ for all t and t'. This means that the voltage of the full model is always below that of the reduced model. A direct consequence of this is that if at time t, the thresholds of both full and reduced models are set to the same value $S > s_0$, the reduced model will be the first of the two to fire. In terms of the maps, this translates into $F_1(t, S) < H_1(t, S)$. Denoting by T_m the shortest interspike interval of the reduced model, i.e. $T_m = \inf\{F_1(t, S) - t : t \geq 0, S \geq s_0\}$, we see that T_m does not depend on τ_v, and $t_{n+1} - t_n \geq T_m \geq \ln[(s_0 + W(s_r, \alpha) - s_r)/(V_r + A - s_r)] > 0$ for any pair of successive discharge times (t_n, t_{n+1}) of the full model (at any value of τ_v).

Now, we compare in more detail the discharge times of the full and reduced models. The discharge times of both models are defined by the following implicit relation:

$$\Phi(t', t, S, \tau_v) \stackrel{\text{def}}{=} s(t', t, S) - \hat{v}(t') - g(t', t, \tau_v) = 0. \tag{26}$$

From the definition of g, setting $\tau_v = 0$ in this equation corresponds to the reduced model. However, this does not imply that the above relation is smooth in $\tau_v = 0$. In fact $\tau_v \to \Phi(t' = t, t, S, \tau_v)$ is not continuous at $\tau_v = 0$. This does not pose a problem in the following, because as reported in the preliminary remark of the previous paragraph, our main interest would be in the range of $t' \geq t + T_m$, and therefore bounded away from $t' = t$.

We denote by $\Theta(t, S, 0) = \min\{t' > t : \Phi(t', t, S, 0) = 0\}$ the discharge time of the reduced model, that is, $\Theta(t, S, 0) = F_1(t, S)$. Our assumptions on model parameters ensure that for $S \geq s_0$, $\Theta(t, S, 0)$ is well defined, and moreover that $\Theta(t, S, 0) \geq t + T_m$. The map $(t', \tau_v) \to g(t', t, \tau_v)$ is of class C^m (m times smoothly differentiable) for any positive integer m, on $[t + T_m/2, +\infty) \times [0, +\infty)$. The same holds for $(t', \tau_v) \to \Phi(t', t, S, \tau_v)$. Moreover, from condition (22) the partial derivative $\partial\Phi/\partial t'$ does not vanish at $(\Theta(t, S, 0), t, S, 0)$. More precisely

$$\frac{\partial\Phi}{\partial t'}(\Theta(t, S, 0), t, S, 0) = \frac{\partial s}{\partial t'}(\Theta(t, S, 0), t, S) - \hat{v}'(\Theta(t, S, 0)), \tag{27}$$

$$\frac{\partial \Phi}{\partial t'}(\Theta(t, S, 0), t, S, 0) < s_r - V_r + A\sqrt{1+\Omega^2}, \tag{28}$$

$$\frac{\partial \Phi}{\partial t'}(\Theta(t, S, 0), t, S, 0) < 0. \tag{29}$$

Given the above conditions, the implicit function theorem yields that there are neighborhoods U and U' of $\tau_v = 0$ and $\Theta(t, S, 0)$ in $[0, +\infty)$ and $[t + T_m/2, +\infty)$, such that for each $\tau_v \in U$, there is a uniquely defined $\Theta(t, S, \tau_v) \in U'$ such that $\Phi(\Theta(t, s, \tau_v), t, s, \tau_v) = 0$. Furthermore $\tau_v \to \Theta(t, S, \tau_v)$ is of class C^m (for any positive integer m) on U.

The above means that the voltage and threshold of the full model cross one another at time $\Theta(t, S, \tau_v)$. The preliminary remark above precludes such intersections at any time t' such that $t < t' < t + T_m$ (in fact, we must have $t' > t + \Theta(t, S, 0) \geq T_m$), so that $\Theta(t, S, \tau_v)$ is indeed the first crossing between the voltage and the threshold following t. In other words we have $\Theta(t, S, \tau_v) = H_1(t, S)$. Combining this with $\Theta(t, S, 0) = F_1(t, S)$, and the smoothness of $\tau_v \to \Theta(t, S, \tau_v)$ establishes that $H_1(t, S) \to F_1(t, S)$ as $\tau_v \to 0$. Finally, given that $H_2(t, S) = s_0 + W(s(H_1(t, S), t, S), \alpha)$, and $F_2(t, S) = s_0 + W(s(F_1(t, S), t, S), \alpha)$, the pointwise convergence of H_2 to F_2, and henceforth that of the full annulus map H to the reduced annulus map F, at fixed (t, S) as $\tau_v \to 0$ follows suit. □

Corollary 1. *The derivatives of H also tend pointwise to those of F as* $\tau_v \to 0$.

Proof. For τ_v sufficiently small, the map $(t, S, \tau_v) \to \Theta(t, S, \tau_v)$ is also of class C^m. This completes the proof. □

5.3. Uniform convergence of the full model to the reduced model

Theorem 2. *Let the maps H and F be defined as above. Let time be rescaled to the threshold time scale* $t \to t/\tau_s$, *and set* $V_r = \mu\tau_v$, $A = a\tau_v/\sqrt{1 + w^2\tau_v^2}$, $\Omega = w\tau_s$, $\cos(\phi) = 1/\sqrt{1 + w^2\tau_v^2}$ *with* $\phi \in [0, \pi/2]$. *As* $\tau_v \to 0$, *while holding* V_r, *A and* ϕ *constant, the map H of the full model converges uniformly to the map F of the reduced model defined above.*

Proof. For $\tau_v > 0$, the function g introduced in Eq. (24) satisfies:

$$g(t', t, \tau_v) < g(t', t, \tau_v') < 0 \quad \text{for } \tau_v > \tau_v', \tag{30}$$

$$-e^{-T_m/\tau_v}(V_r + A) < g(\Theta(t, S, \tau_v), t, \tau_v) < 0. \tag{31}$$

From the first inequality, we derive that $\tau_v \to \Theta(t, S, \tau_v)$ is monotonic increasing, that is $\Theta(t, S, \tau_v) > \Theta(t, S, \tau_v')$ for $\tau_v > \tau_v'$. From the second inequalities, we obtain that the crossing time $\Theta(t, S, \tau_v)$ is between $\Theta(t, S, 0)$ (the crossing time of the reduced model) and that of the threshold through $\tilde{v}(t) = \hat{v}(t) - e^{-T_m/\tau_v}(V_r + A)$. We denote this latter time as $\tilde{\Theta}(t, S, \tau_v)$. Now, under condition (22), we have that for τ_v sufficiently small

$$s_r - V_r + A\sqrt{1+\Omega^2} + e^{-T_m/\tau_v}(V_r + A) < 0, \tag{32}$$

so that:

$$0 < \Theta(t, S, \tau_v) - \Theta(t, S, 0) < \tilde{\Theta}(t, S, \tau_v) - \Theta(t, S, 0) < b(\tau_v), \tag{33}$$

where

$$b(\tau_v) \stackrel{\text{def}}{=} \frac{e^{-T_m/\tau_v}(V_r + A)}{V_r + s_r - A\sqrt{1+\Omega^2} - e^{-T_m/\tau_v}(V_r + A)}, \tag{34}$$

tends to zero as $\tau_v \to 0$.

Thus, we have $H_1(t, S) = \Theta(t, S, \tau_v) \to F_1(t, S) = \Theta(t, S, 0)$ monotonically uniformly as $\tau_v \to 0$ and the right hand side of inequality (33) provides an upper bound for the speed of the convergence. Using (33), we obtain the following bound for the differences between the thresholds at the discharge times of the reduced and full models:

$$0 \leq s[\Theta(t, S, 0), t, S] - s[\Theta(t, S, \tau_v), t, S] \leq (S_M - s_r)\, \mathrm{e}^{-T_m}[1 - \mathrm{e}^{b(\tau_v)}], \tag{35}$$

where $S_M = s_0 + W(V_r + A\sqrt{1+\Omega^2}, \alpha)$, does not depend on (t, S). This inequality shows that $(t, S) \to s[\Theta(t, S, \tau_v), t, S]$ converges uniformly to $(t, S) \to s[\Theta(t, S, 0), t, S]$ as $\tau_v \to 0$. This yields uniform convergence of H_2 to F_2, as

$$0 \leq F_2(t, S) - H_2(t, S) \leq K(S_M - s_r)\, \mathrm{e}^{-T_m}[1 - \mathrm{e}^{b(\tau_v)}], \tag{36}$$

where

$$K = \max\left\{ \frac{\partial W}{\partial s}(s, \alpha) : s \in [s_0 + W(s_r, \alpha), V_r + A\sqrt{1+\Omega^2}] \right\}.$$

Furthermore, in the same way as for H_1 to F_1, the convergence of H_2 to F_2 is monotonic (i.e. H_2 increases to F_2 as $\tau_v \to 0$) because $s \to W(s, \alpha)$ is monotonic increasing, $t' \to s(t', t, S)$ is monotonic decreasing, and $\tau_v \to \Theta(t, S, \tau_v)$ is monotonic increasing. This completes the proof of the uniform convergence of H to F as $\tau_v \to 0$. □

We have actually proved a stronger result in that $\|F - H\|$ decreases monotonically to zero as $\tau_v \to 0$, where the $\|\cdot\|$ represents the supremum norm for $(t, S) \in [0, T] \times [s_0 + W(s_r, \alpha), S_M]$.

5.4. Geometrical interpretation of the reduction

We now provide a geometrical interpretation of the above results to show how the annulus map is transformed into a circle map as $\tau_v \to 0$. The annulus map $\tilde{F}$ of the reduced model maps the whole annulus into the subset $C = \{(\theta, S) : S = s_0 + W(\hat{v}(\theta/\Omega), \alpha)\}$ (Section 5.1). The set C is a circle-like subset winding around the "hole" in the middle of the annulus. Defining $C(\tau_v) = \{(\theta, S) : S = s_0 + W(\tilde{v}(\theta/\Omega), \alpha)\}$ by substituting $\tilde{v}$ for $\hat{v}$ in the definition of C, we obtain another circle-like subset of the annulus that lies "inside" C, in the sense that at fixed angle θ, the radius of $C(\tau_v)$ is smaller than that of C. In this way, the region, denoted by $\Xi(\tau_v)$ is between $C(\tau_v)$ from inside and C from outside, is itself annulus-like. The annulus map $\tilde{H}$ of the full model maps the whole annulus into $\Xi(\tau_v)$. As $\tau_v \to 0$, the lower border $C(\tau_v)$ of $\Xi(\tau_v)$ approaches the upper border C uniformly in (θ, S), so that the two-dimensional domain $\Xi(\tau_v)$ shrinks into the one-dimensional graph C, accounting for the transformation of the full model into the reduced model described by the iterates of a circle map.

Finally, to ensure that H inherits some of the dynamics of F when τ_v is sufficiently small, we show that partial derivatives of H with respect to t and S converge uniformly to the partial derivatives of F as $\tau_v \to 0$. The expressions for the partial derivatives of H_1 and F_1 with respect to t and S can be obtained from the implicit function theorem applied to Φ (Eq. (26)). The uniform convergence of H_1 to F_1 together with Eq. (31), ensure that $\partial H_1/\partial t$ and $\partial H_1/\partial S$ converge uniformly to $\partial F_1/\partial t$ and $\partial F_1/\partial S$ for $(t, S) \in [0, T] \times [s_0 + W(s_r, \alpha), S_M]$ as $\tau_v \to 0$. The uniform convergence of $\partial H_2/\partial t$ and $\partial H_2/\partial S$ to $\partial F_2/\partial t$ and $\partial F_2/\partial S$ is obtained in a similar way.

In conclusion, we have that $\|F - H\| + \|\mathrm{d}F - \mathrm{d}H\| \to 0$ as $\tau_v \to 0$, where $\mathrm{d}F(t, S)$ and $\mathrm{d}H(t, S)$ are linear operators on the plane defined by the differentials of F and H with the second norm above computed as

$$\|\mathrm{d}F - \mathrm{d}H\| = \sup_{(t,S)\in[0,T]\times[s_0+W(s_r,\alpha),S_M]} \|\|\mathrm{d}F(t, S) - \mathrm{d}H(t, S)\|\|$$

$$\|\|(\mathrm{d}F(t,S)-\mathrm{d}H(t,S))\|\| = \sup_{\max(|l_1|,|l_2|)=1} \|(\mathrm{d}F(t,S)-\mathrm{d}H(t,S))(l_1,l_2)\|.$$

One can thus consider the map H associated with the full model as a regular perturbation of the map F associated with the reduced model. This implies some similarity between the dynamics of the full and reduced models. For instance if for some parameter α, F has a hyperbolic fixed point or periodic orbit, then so would H for sufficiently small τ_v. Furthermore, the corresponding fixed point or periodic orbit of H would be close to that of F. In general, if the dynamics of the reduced model are structurally stable on the annulus, then for τ_v sufficiently small, the dynamics of the full and reduced models would be qualitatively similar. In the same way, if for some α_c, the reduced model undergoes a codimension one bifurcation, one expects to find a similar bifurcation for a nearby $\alpha = \alpha_c(\tau_v)$ for all τ_v sufficiently small. For more complex dynamics, our numerical investigations suggest that the similarity between full and reduced models is also present in the regimes where the reduced model displays chaotic dynamics (these are identified numerically from the sign of the Lyapunov exponent). The reduction is thus a valid means to investigate the mechanisms underlying chaotic dynamics in the full model.

5.5. *Practical consideration on the approximation with the circle map*

The bounds on the distance between the map of the full model and that of the reduced model are given in Eqs. (33) and (36). The key quantity that ensures that these bounds tend to zero as $\tau_v \to 0$ is e^{-T_m/τ_v}. Having $\mathrm{e}^{-T_m/\tau_v} < \varepsilon$ ensures that $\|F - H\| < c\varepsilon$ for some constant c that is independent from τ_v. So the condition for H to be close to F with the precision $c\varepsilon$ is verified as soon as $\tau_v < -T_m \ln \varepsilon$. We remind that T_m is the shortest interdischarge interval for the reduced model, computed over all initial conditions on the annulus, that is, $T_m = \inf\{F_1(t,S) - t : t \geq 0, S \geq s_0 + W(s_r,\alpha)\}$. Thus T_m is longer than the time required for the threshold initiated at the lowest threshold level $s_0 + W(s_r,\alpha)$ to reach $V_r + A$, the highest voltage value. In other words, we have a lower bound for T_m which is: $T_m \geq T^* = -\ln[(s_0 + W(s_r,\alpha) - s_r)/(V_r + A - s_r)] > 0$. The condition $\tau_v < -T^* \ln \varepsilon$, ensures that the distance between F and H is smaller than $c\varepsilon$. As T^* can be computed directly from model parameters, this relation can be used in practice to obtain an upper bound for the distance between full and reduced models.

It is possible to improve on this first approximation by limiting the set over which the minimal interdischarge interval is computed from the full annulus to the set $\Xi(\tau_v)$ (comprised between $C(\tau_v)$ and C). Indeed, as argued previously, the iteration of $\tilde{H}$ sends the annulus into this set, so that one can limit the comparison of the action of $\tilde{F}$ and $\tilde{H}$ to the set $\Xi(\tau_v)$. We denote by T'_m this minimal value to distinguish it from the previous one.

The restriction from the annulus to $\Xi(\tau_v)$ increases the lowest admissible threshold from $s_0 + W(s_r,\alpha)$ to $s_0 + W(V_r - A - \mathrm{e}^{-T_m/\tau_v}(V_r + A),\alpha)$. From this we derive that:

$$T'_m \geq \ln\left\{\frac{s_0 + W(V_r - A - \mathrm{e}^{-T_m/\tau_v}(V_r + A),\alpha) - s_r}{V_r + A - s_r}\right\} \geq T^{**}(\tau_v),$$

where

$$T^{**}(\tau_v) = \ln\left\{\frac{s_0 + W(V_r - A - \mathrm{e}^{-T^*/\tau_v}(V_r + A),\alpha) - s_r}{V_r + A - s_r}\right\}.$$

The condition $\tau_v < -T^{**}(\tau_v)\ln(\varepsilon)$ ensures that on $\Xi(\tau_v)$ the map of the reduced model approximates that of the full model with a precision better than $c\varepsilon$. We have $T^{**}(\tau_v) > T^*$, so that the new condition reveals that the

approximation by the circle map holds to a precision $c\varepsilon$ over a wider range of τ_v than the one derived from T^*. In this sense, the restriction of the set yields an improvement.

5.6. Lyapunov exponent of the reduced model

We have shown that the reduced model can be described by iterates of a one-dimensional map. Here again, as in Section 3, we can either derive the Lyapunov exponents associated to this map, or, as before, analyze the growth rate of small perturbations to the model variables. We once again adopt the second approach. The expressions are presented in Appendix A.

5.7. The mechanism for chaos: relation with non-monotonic circle maps

The reduction of the model is possible only under certain hypotheses on the voltage and threshold time scales. Theoretical arguments suggest that despite these simplifying assumptions, the reduced model can capture the main scenarios of transition to chaos observed in the full model. This is verified using numerical simulations: Fig. 3 illustrates the similarity between the two models. Fig. 3a shows the bifurcation diagram while Fig. 3b shows the Lyapunov exponent of the reduced model when the parameter α is increased. As in Fig. 2, transitions to chaos in the reduced model are associated with period doubling and halving cascades as well as tangent bifurcations. In this sense, the reduced model reproduces the main scenarios observed for the full model and constitutes a satisfactory simplification.

The contribution of this reduction is that the dynamics of the one-dimensional model correspond to those of circle maps, that is, of a well understood class of systems. Therefore, we can take advantage of this, to determine how the increase in the parameter α can lead to chaos. We now study the effects of different functional forms for the function W on the dynamics exhibited by the model.

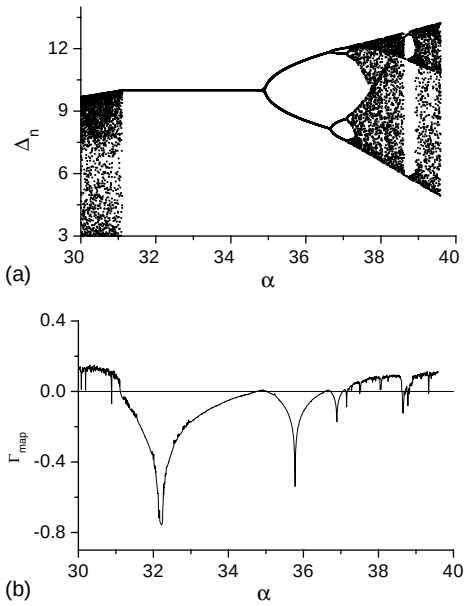

Fig. 3. (a) ISI Δ_n as a function of α illustrating the complex dynamics displayed by the reduced model. It displays similar dynamics to the full model. (b) Lyapunov exponent Γ_{map} of the reduced model. Γ_{map} is positive for certain value of α indicative of chaotic dynamics. Parameter values are the same as in Fig. 2.

6. The circle map is monotonic for sublinear fatigue, and non-monotonic for sufficiently supralinear fatigue

In this section, we examine the dependence of the circle map on the rate of increase of the fatigue function W. Roughly speaking, when W increases at most linearly, then the map is always one-to-one. Conversely, when $W[s, \alpha]$ increases as s^β, then the map is non-monotonic for $\beta > 1$ large enough. The exact value of β is shown to depend on the system parameters.

The circle map $\tilde{f}$ is of degree-one as $f(t + T) = f(t) + nT$ for $n = 1$. Therefore $\tilde{f}$ is one-to-one if and only if it is monotonic increasing. When this is the case, iterations of $\tilde{f}$ cannot produce chaos. Using this observation, we prove that when the threshold fatigue $W[s, \alpha]$ does not increase rapidly enough in s, chaotic dynamics cannot occur. The importance of this result is in that it does not depend on model parameters as long as one assumes that condition (22) is satisfied, which was the case throughout the reduction procedure. Next, we investigate necessary conditions for the occurrence of chaos. These depend more explicitly on parameters, in the sense that the minimal rate of increase of W to destroy monotonicity of f depends on s_r, V_r, A and Ω, and the minimal value of α at which this happens depends on these and s_0.

One way to interpret the dynamics of the reduced model is to consider that, after each discharge, the threshold is reset at $\hat{v}_h(t) = s_0 + W(\hat{v}(t), \alpha)$ and then decays exponentially until reaching $\hat{v}$ at some time $t' > t$ ($\hat{v}(t)$ is defined in Eq. (15)). A necessary condition for a discharge to occur at a time t is that the threshold cross $\hat{v}$ from above at t. In other words, the slope of the threshold at the crossing must be smaller than the slope of the voltage. Now, the slope of the threshold equals $s_r - s$, which at the time of crossing equals $s_r - \hat{v}$. With this, the necessary condition for a discharge to occur at t reads:

$$s_r - \hat{v} \leq \hat{v}'. \tag{37}$$

This inequality is satisfied when condition (22) holds. Hence, it holds for all reduced models considered in this work, and we assume that it is valid throughout this section as well. In other words, we deal with circle maps that are onto. This is of prime importance. Indeed, for the sinusoidally forced standard LIF, there are parameter ranges such that the circle map is not monotonic. However, in these cases, the map is not onto, and when it is restricted to its domain, it becomes monotonic [19]. Such a restriction is not possible in the situations we consider below because the map is onto, and the lack of monotonicity cannot be avoided by restricting the domain.

In the degree-one circle maps we consider, chaos cannot occur if the map is monotonic. Therefore a sufficient condition to exclude chaos is to show that the map is monotonic and, conversely, a necessary condition for the occurrence of chaos is for the map to be non-monotonic. Equivalently, we can restate these conditions as follows: a sufficient condition to exclude chaos is that the map be one-to-one and a necessary condition for chaos is the existence of two points $t_1 < t_2$ in $[0, T)$ with $f(t_1) = f(t_2)$. So we examine first necessary and sufficient conditions for the map to be one-to-one.

A necessary and sufficient condition for the circle map to be one-to-one is that any threshold curve $t \to s(t, t_0, S)$ cross the reset curve $\hat{v}_h$ at a single point. If there is a threshold curve crossing $\hat{v}_h$ at two distinct points $t_1 < t_2$ in $[0, T)$, then we have $s(t, t_1, \hat{v}_h(t_1)) = s(t, t_2, \hat{v}_h(t_2))$ for all t, notably at the crossing between the threshold and the voltage $\hat{v}$, so that $f(t_1) = f(t_2)$, and the map is not one-to-one. Conversely, when the circle map is not one-to-one, there are at least two points $t_1 < t_2$ in $[0, T)$ with $f(t_1) = f(t_2)$. This means that the thresholds $t \to s(t, t_1, \hat{v}_h(t_1))$ and $t \to s(t, t_2, \hat{v}_h(t_2))$ intersect one another as they cross the voltage curve $t \to \hat{v}(t)$ at the same point. Now, the threshold curves being the solutions of the same scalar ordinary differential equation, that they intersect at one point implies that they represent the same solution. In other words, $s(t, t_1, \hat{v}_h(t_1)) = s(t, t_2, \hat{v}_h(t_2))$, which shows this threshold curve intersects the voltage at least two points t_1 and t_2. This relation shows that when the circle map is not one-to-one, there is a threshold curve crossing $\hat{v}_h(t)$ at at least two distinct points.

We can translate these conditions in terms of the derivatives of the voltage and the reset voltage. More precisely, a sufficient condition for the circle map to be one-to-one is that the slope of the threshold on the reset curve $\hat{v}_h$ is lower than the slope of $\hat{v}_h$ at all crossings. Given that the slope of the threshold at the crossing is given by $s_r - s = s_r - \hat{v}_h$, this conditions reads:

$$s_r - \hat{v}_h < \hat{v}_h'. \tag{38}$$

In summary, assuming that (37) holds, inequality (38) is a sufficient condition for the circle map to be one-to-one: it is a sufficient condition to rule out chaos.

Conversely, a sufficient condition for the map not to be one-to-one is that there exist some $t^* \in [0, T)$ such that the threshold crosses from below $\hat{v}_h$ at time t^*, with derivatives satisfying:

$$s_r - \hat{v}_h(t^*) > \hat{v}_h'(t^*). \tag{39}$$

In fact, at such a point t^*, the map f is decreasing, i.e. $f'(t^*) < 0$. In this way, the range of t^* such that inequality (39) holds corresponds to the range where f is decreasing. Its lower and upper borders correspond to the extrema of f. This is why the existence of t^* ensures that the map is no longer monotonic increasing, but also exhibits monotonic decreasing regions.

We remind that the typical fatigue functions used in this work are $W(s, \alpha) = \alpha(s - s_r)$ and $W(s, \alpha) = \exp(\alpha(s - s_r)) - 1$. Generally, we rewrite the fatigue function as $G(\alpha(s - s_r)) = W(s, \alpha)$. The function G is non-decreasing (i.e. $G' \geq 0$) and satisfies $G(0) = 0$. Denoting $u = \hat{v} - s_r$, then condition (37) translates into:

$$-u \leq u', \tag{40}$$

and the conditions (38) and (39) hold depending on whether the following quantity R is positive at all times, or whether there exists $t^* \in [0, T)$ such that it is negative:

$$R = s_0 - s_r + G(\alpha u) + \alpha u' G'(\alpha u). \tag{41}$$

6.1. Sufficient condition for the map to be monotonic increasing

Theorem 3. *Let W be linear or concave down. Then $R > 0$ is always satisfied.*

Proof. Using inequality (40), the monotonicity of G, and the fact that $s_0 > s_r$, we have

$$R > G(\alpha u) - \alpha u G'(\alpha u). \tag{42}$$

Therefore, a sufficient condition for $R > 0$ is $G(\alpha u) \geq \alpha u G'(\alpha u)$. Clearly this is satisfied when G is linear. When G is concave down, G' is decreasing, so that $G(\alpha u) = \int_0^{\alpha u} G'(x)\,\mathrm{d}x \geq \int_0^{\alpha u} G'(\alpha u)\,\mathrm{d}x = \alpha u G'(\alpha u)$, which is exactly the inequality above. In conclusion, we have established that the circle map is one-to-one and hence monotonic increasing when W is linear or concave down (referred to as sublinear). □

6.2. Sufficient condition for the map to become non-monotonic for α large regardless of model parameters

Theorem 4. *Let R be defined as above $G(x) = \exp(x) - 1$. Then there exists at least one t^* and α such that $R < 0$ and thus the circle map f is non-monotonic.*

Proof. At $\alpha = 0$, we have $R = s_0 - s_r > 0$ so that the circle map is monotonic. Therefore, $R < 0$ may occur only for α large. Furthermore, examining the terms in R (Eq. (41)) reveals that the first two terms are positive as is

$\alpha G'(\alpha u)$. Thus R can become negative only at a time t^* such that $u'(t^*) < 0$. So in fact, we examine whether at some fixed t such that $u'(t) < 0$ increasing α can render R negative. We have thus limited the domain of t.

We introduce the following notations: $x = \alpha u$, $M = s_r - s_0 > 0$, and $L = -u'(t)/u(t)$. For t such that $u'(t) < 0$, we have $0 < L \leq L_M < 1$ with $L_M = A\Omega/\sqrt{(V_r - s_r)^2 - A^2}$ and $L = L_M$ at t such that $\sin(\Omega t - \phi) = -A/(V_r - s_r)$. We define $x \to i(x)$ for $x \geq 0$ as

$$i(x) = LxG'(x) - G(x) - M. \tag{43}$$

Then showing that $R < 0$ for some t^* and α large enough is equivalent to showing that $i(x) > 0$ for $x > 0$ large enough with $L = -u'(t^*)/u(t^*)$.

For $G(x) = \exp(x) - 1$, we have $i(x) = \exp(x)(Lx - 1) + 1 - M$, which is a monotonic increasing function tending to $+\infty$ as $x \to +\infty$. Thus for each L, there exists a unique $x^* > 0$, such that $i(x^*) = 0$ and $i(x) > 0$ if and only if $x > x^*$. This means that for any t such that $u'(t) < 0$, there is α^* such that for $\alpha > \alpha^*$, we have $R < 0$. □

This establishes that for W exponential, the circle map becomes non-monotonic for α large enough, and that this holds regardless of the choice of the model parameters as long as condition (22) holds. Furthermore, the range of t where lifts of the circle map are decreasing broadens with α to cover all t such that $u'(t) < 0$, that is t in the union of $(\phi + T/4 + kT, \phi + 3T/4 + kT)$ for all integers k. The two previous analyzes are concerned with the two extreme situations where, irrespective of parameters (other than α), the map remains either monotonic for all α, or conversely, becomes non-monotonic for α sufficiently large. The first holds for W linear and sublinear and the second for W exponential. Here, we examine a class of intermediate supralinear functions. This completes the proof and sheds light on the transition between the two extreme cases.

6.3. Sufficient condition for the map to become non-monotonic for α large depending on model parameters

Theorem 5. *Let G be such that $G(x) - x^\beta = \eta(x)$, where $\beta > 1$ is a real number and η is a smooth function satisfying $\eta(x) \to 0$ and $\eta'(x) \to 0$ as $x \to +\infty$. Then the map f is non-monotonic for α large enough.*

Proof. In this way, for x large, G is close to a convex monotonic increasing function with a power growth rate x^β. Substituting this into i (Eq. (43)) yields

$$i(x) = (\beta L - 1)x^\beta - M - \eta(x) + Lx\eta'(x). \tag{44}$$

Given that $\beta > 1$, the first term is the dominating term as $x \to +\infty$, and $\beta L - 1$ determines the sign of i for large x. If $\beta \leq 1/L_M$, we have $i < 0$, so that for large α, the circle map is monotonic increasing. This relation shows that not only sublinear and linear fatigues lead to monotonic circle maps, but that this also extends to supralinear fatigues with low power growth rates. Only, in this case, the upper limit growth rate depends on L_M and therefore on model parameters. There is not a value $\beta > 1$ such that for all parameters, one would expect to have monotonic increasing circle maps at all values of α. Changing the parameter values modifies L_M and therefore the limiting value $\beta_m = 1/L_M$. In other words, for a given $\beta > 1$, there will be some parameters that would yield monotonic circle maps at all α, and other parameters for which the circle map becomes non-monotonic for large α.

For $\beta > \beta_m$, the function i becomes positive for x large enough and tends to $+\infty$ as $x \to +\infty$. In this case, for α large enough, the circle map is no longer monotonic. The range of t for which any lift of the circle map is decreasing depends on the value of β, and is more restricted than for exponential fatigue, even as $\alpha \to +\infty$. For the power growth rate, this asymptotic range is that of t such that $L > 1/\beta$, whereas for the exponential fatigue it is t such that $L > 0$. Increasing β widens this range towards that of the exponential fatigue. □

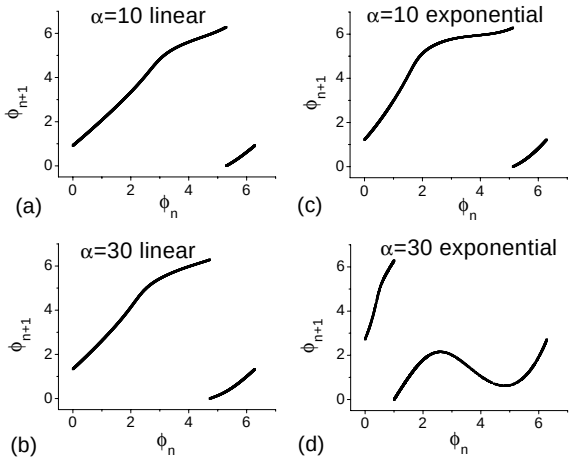

Fig. 4. The circle map $f(t)$ for different values of α and different functional forms for W. The circle map for $W[s,\alpha] = \alpha * (s - s_r)$ and $\alpha = 10$ (a) and $\alpha = 30$ (b). The circle map for $W[s,\alpha] = \exp(\alpha * (s - s_r)) - 1$ and $\alpha = 10$ (c) and $\alpha = 30$ (d). Other parameter values are the same as in Fig. 2.

6.4. Summary of results

In summary, our analysis focussed on conditions on the growth rate of the fatigue function that would ensure either monotonic increasing circle maps at all α (W sublinear, linear and weakly supralinear power function), or would lead to a loss of monotonicity for α large enough (W strongly supralinear power function and exponential). Chaos can only occur in the latter case. Numerical simulations confirm that it does for some W such as the exponential one.

6.5. Examples of circle maps

We end this section by providing several examples of the circle maps for different fatigue functions W and α. The left column in Fig. 4 illustrates the case of linear fatigue $W(s,\alpha) = \alpha(s - s_r)$ for $\alpha = 10$ and 30 (top and bottom). The panels of the right column represent the case of W with exponential $W(s,\alpha) = \exp(\alpha(s - s_r)) - 1$ for the same values of α. As expected, in all cases the maps are monotonic for α small (upper row). For W linear, it remains so at larger α, but in the other case, the map develops a local extremum: it is no longer monotonic. The map in the lower right panel actually leads to chaotic dynamics as seen in Fig. 3. We also note that it is possible to obtain chaotic dynamics for sigmoidal fatigue functions (data not shown).

7. Discussion

The periodically forced standard LIF cannot produce chaotic firing. Variants of this model have been proposed that overcome this issue. Modifications leading to these variants were not necessarily motivated by biologically plausible mechanisms. For instance, one approach that renders the LIF capable of exhibiting chaotic dynamics is to add the periodic modulation to the postdischarge resetting voltage rather than as an injected current [10]. Such variants of the LIF have been successful in reproducing the behavior of specific physical, chemical and biological systems [2,14]. However, our concern was the case of sensory neurons for which the influence of periodic sensory stimulation is not necessarily limited to postdischarge membrane potential resetting. Different mechanisms may

underlie the complex behavior of periodically forced neurons. For this reason, our study focussed on a specific biologically plausible property, namely threshold fatigue.

Our specific purpose in this paper was to show that threshold fatigue can be one source of chaos in neurons. The mechanism implemented in the model differs from those included in previous variants of the LIF that produce chaos. It is legitimate to consider whether this difference is merely at the level of the model or whether it has also implications in terms of the dynamics. In other words, the question is whether the LIF with threshold fatigue presents the same dynamics as those of other variants of the LIF that display chaos, or whether this model can potentially exhibit novel dynamics. At this time, this is an open question, however, it is possible to discuss it based upon the dynamical characteristics of the models.

The dynamics of the periodically forced standard LIF and variants with periodically modulated threshold or resetting voltage can be described in terms of iterates of circle maps. We showed that a similar description holds for the LIF with threshold fatigue, when the voltage time scale is substantially smaller than the threshold time scale. The circle map corresponding to the standard LIF is monotonically increasing, at least when the map is restricted to its range. This precludes chaotic dynamics. For the modified LIF where the periodic modulation is implemented in the voltage resetting value, the situation is different. The corresponding circle map is no longer necessarily monotonic: it is possible to have situations where the map is no longer one-to-one. For these maps the dynamics can be chaotic [10].

We clarify the relation between the LIF with threshold fatigue and the other LIF variants. It is possible to consider variants of the LIF, where the periodic modulation is imposed simultaneously on both the postdischarge voltage and the threshold (see e.g. [10]). The dynamics of the voltage between successive firings are then supposed to be exempt of any periodic forcing and follow an exponential function connecting the postdischarge voltage curve to the threshold curve. Clearly the successive discharge phases of such models are described by iterates of circle maps. When the amplitude of threshold modulation is lower than or equal to that of the postdischarge reset, the circle map is orientation preserving or can be restricted to a monotonic map. Chaotic dynamics are thus not possible. Conversely, when it is the modulation amplitude of the postdischarge voltage that is larger, the circle map is not necessarily monotonic, and the dynamics can be chaotic.

The LIF variant with constant threshold and modulated resetting is the extreme case of this model. The standard LIF, on the other hand, is similar to the case where both threshold and reset voltage are modulated with the same amplitude. Our reduction of the LIF with threshold fatigue shows that when the voltage recovery is substantially faster than the threshold decay, the dynamics of the LIF with threshold fatigue is also similar to the general class of model described above. In contrast with other LIF models, in our approximation it is the threshold, rather than the voltage that is reset after each discharge. In the approximated model, the threshold exponentially decays between two periodic functions (the voltage and its reset value). The parameter α, representing threshold fatigue, controls the ratio of the amplitudes of these functions. When α is large, the amplitude of the postdischarge reset function becomes the larger of the two. Thus, the circle map is not necessarily one-to-one in this case and chaotic dynamics become possible. Although chaotic dynamics were not observed for a linear fatigue function, they were observed when it was sufficiently non-linear.

The remaining issue is whether in the general case, for arbitrary voltage and threshold time scales, where the dynamics of the model cannot be reduced to iterates of a circle map, novel dynamics can occur. The dynamics of circle maps are essentially characterized by their rotation number. When the map is monotonic, the rotation number is uniquely defined regardless of the initial condition. Rational rotation numbers define the phase locked regimes and irrational rotation numbers characterize quasiperiodic or strange non-chaotic dynamics. When the map is no longer one-to-one, the rotation numbers depend on the initial condition and therefore form an interval (the rotation interval) depending on the initial conditions, and still carry on valuable information about the long term dynamics of the system. For instance, when the rotation interval is not reduced to a single point, chaos can occur [6]. So one can wonder whether a quantity similar to the rotation number can also be defined for the

annulus map associated with the periodically forced LIF with threshold fatigue, and also whether this quantity would impose similar restrictions on the dynamics of the map. It is possible to provide partial answers to these questions.

The annulus map associated with the periodically forced LIF with threshold fatigue is not arbitrary. It is in fact a twist map of the annulus [22], because for fixed t, the map $s \to t' = H_1(t, s)$ (defined Eqs. (8)) is monotonic increasing. This is easily understood in biological terms: given two neurons subject to the same periodic stimulation, and having discharged simultaneously, the one with the lower postdischarge threshold of the two will fire sooner than the other. This property severely constrains the dynamics of the annulus map, however, it does not reduce it to that of a circle map. For instance, rotation numbers can be defined for twist circle maps, however, they do not necessarily form an interval [22], a situation that would be precluded for circle maps. In terms of the neuronal model, this example indicates that the LIF with threshold fatigue may display dynamics that have no counter part in other LIF variants that can be analyzed in terms of circle map iterates. In our opinion, this opens interesting direction for future research. Systematic exploration of the dynamics of the LIF with threshold fatigue, and its associated twist annulus map should clarify whether indeed neuronal membranes with strong fatigue and consequently adaptation properties, may exhibit specific dynamics in response to periodic forcing that do not exist in non-adapting membranes.

Early experiments performed by Blair and Erlanger in 1930s, were aimed to quantify the all-or-none response of nerve fibers [5]. These experiments consisted in administering periodic shocks to axons and monitoring their response. In general, the time interval separating two successive stimuli was set large enough for the nerve to completely recover between two shocks. However, controls were run with shorter periods. In these [5] the authors reported what they referred to as “apparently random appearance of responses” and proposed that development of “phase differences between the rhythmic process of recovery from activity and the development of fatigue” could be responsible for these complex behavior. It is not possible to confirm with certainty that the dynamics observed by these authors would fit the present day definition of chaos. Nevertheless, their description remains remarkable in the sense that they did not attribute the irregularity of the response to noise alone. They explicitly recognized that another mechanism based upon differences in time scales could be involved. In other words, they seem to have been aware that non-random effects could produce apparently random responses in axons. To our knowledge, these experimental results are the first evidence that threshold fatigue could lead to complex dynamics in periodically forced neurons.

Acknowledgements

KP would like to thank Patrice Le Calvez for helpful discussions on maps of the annulus. This research was supported by NSERC (MJC and AL).

Appendix A.

A.1. Derivation of the Lyapunov exponents of the full model

For the standard LIF, it is only necessary to consider a voltage solution $v(t)$ and a perturbed solution $v_p(t)$ with $\delta v(t) \equiv v_p(t) - v(t)$. It is then possible to derive a recurrence relation between $\delta v(t_{n+1})$ and $\delta v(t_n)$ keeping only first order terms and thus to define a Lyapunov exponent [10]. In our case however, we must also consider an unperturbed threshold solution $s(t)$ and a perturbed threshold solution $s_p(t)$ with $\delta s(t) \equiv s_p(t) - s(t)$. The essence of the method is to follow the temporal evolution of both these small perturbations.

Let us assume that there is a small perturbation $\delta X(0) = (\delta v(0), \delta s(0))^{\mathrm{T}}$ (where the superscript T denotes vector transposition) on an initial condition $X(0) = (v(0), s(0))^{\mathrm{T}}$. If no firing occurs in the time interval $[0, t]$, then the initial perturbation evolves to the value:

$$\delta X(t) = \begin{pmatrix} \delta v(t) \\ \delta s(t) \end{pmatrix} = \begin{pmatrix} \mathrm{e}^{-t/\tau_v} & 0 \\ 0 & \mathrm{e}^{-t/\tau_s} \end{pmatrix} \begin{pmatrix} \delta v(0) \\ \delta s(0) \end{pmatrix} \equiv D_t \delta X(0). \tag{A.1}$$

If there is a single discharge at a time t_1 in $[0, t]$, then we have:

$$\delta X(t) = D_{t-t_1} A_{t_1} D_{t_1} \delta X(0), \tag{A.2}$$

where

$$A_t = \begin{pmatrix} \alpha_t & -\alpha_t \\ -\beta_t & \beta_t + \gamma_t \end{pmatrix} \tag{A.3}$$

with the matrix entries given by

$$\alpha_t = \frac{-(v_0/\tau_v) + \mu + a \sin(wt)}{s(t)[(1/\tau_s) - (1/\tau_v)] - (s_r/\tau_s) + \mu + a \sin(wt)}, \tag{A.4}$$

$$\beta_t = \frac{(s_r - s(t))W'[s(t), \alpha] + s_0 + W[s(t), \alpha]}{s(t)[1 - (\tau_s/\tau_v)] - s_r + \mu\tau_s + a\tau_s \sin(wt)}, \tag{A.5}$$

$$\gamma_t = W'[s(t), \alpha]. \tag{A.6}$$

The matrix A is related to the reset of both voltage and threshold. The derivation of these expressions is given below. Prior to that, we complete the estimation of the Lyapunov exponents. With the same notations as above, the general case where there are n discharges at times $0 \le t_1 < \cdots < t_n \le t$ is given by

$$\delta X(t) = D_{t-t_n} A_{t_n} D_{t_n - t_{n-1}} \cdots D_{t_2 - t_1} A_{t_1} D_{t_1} \delta X(0). \tag{A.7}$$

The Lyapunov exponents measure the growth or decay rates of this quantity and are defined as

$$\lambda_i = \lim_{t \to +\infty} \frac{1}{t} \log\left(\frac{\|\delta X(t)\|}{\|\delta X(0)\|} \right). \tag{A.8}$$

Practically, it is convenient to estimate the Lyapunov exponent by starting and ending the computation at discharge times, that is $t_1 = 0$, and $t = t_n$. In this way, the impact of the perturbation is estimated at successive discharge times, and we have a discrete-time relation instead of Eq. (A.7):

$$\delta X_n = \delta X(t_n), \tag{A.9}$$

$$\delta X_n = D_{t_n - t_{n-1}} A_{t_{n-1}} \cdots D_{t_2 - t_1} A_{t_1} \delta X(0), \tag{A.10}$$

$$\delta X_n \equiv M_n \delta X_0. \tag{A.11}$$

Then, the two Lyapunov exponents of the model can be defined as

$$\lambda = \lim_{n \to +\infty} \frac{1}{2n} \log(\lambda_n), \tag{A.12}$$

$$\mu = \lim_{n \to +\infty} \frac{1}{2n} \log(\mu_n), \tag{A.13}$$

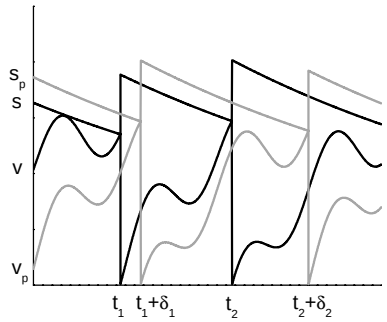

Fig. 5. Illustration of the method for calculating the Lyapunov exponents of the model given in Eqs. (1)–(4). The unperturbed solutions $v(t)$ and $s(t)$ intersect at times t_n while the perturbed solutions $v_p(t)$ and $s_p(t)$ intersect at times $t_n + \delta_n$. One must track the time evolution of the perturbations $\delta s(t) \equiv s_p(t) - s(t)$ and $\delta v(t) = v_p(t) - v(t)$ in order to compute the Lyapunov exponents as explained in the text.

where λ_n and μ_n are the eigenvalues of the symmetrical matrix $M_n^{\mathrm{T}} M_n$. Denoting $m_n = D_{t_{n+1}-t_n} A_{t_n}$, we see that M_n can be computed along the solution as $M_{n+1} = m_n M_n$ for $n \geq 1$ with M_1 set to the identity matrix. In this way, we have a method to estimate numerically the Lyapunov exponents of the system from simulations.

To finish, there remains the derivation of the entries of the matrix A_t. Without loss of generality, we present the analysis in the case of the first discharge at time t_1. The unperturbed solutions $v(t)$ and $s(t)$ intersect at times t_1 while the perturbed solutions $v_p(t)$ and $s_p(t)$ intersect at times $\{t_1 + \delta_1\}$. The situation is illustrated in Fig. 5.

The goal is to derive an expression for $[\delta v(\{t_1 + \delta_1\}^+), \delta s(\{t_1 + \delta_1\}^+)]$ as a function of $[\delta v(t_1), \delta s(t_1)]$ keeping only first order terms with $\delta s(t) \equiv s_p(t) - s(t)$ and $\delta v(t) \equiv v_p(t) - v(t)$. At time $t_1 + \delta_1$, we have:

$$\begin{aligned} &0 = s_p(t_1 + \delta_1) - v_p(t_1 + \delta_1), \qquad 0 \approx s_p(t_1) + \delta_1 \dot{s}_p(t_1) - v_p(t_1) - \delta_1 \dot{v}_p(t_1), \\ &0 \approx \delta s(t_1) - \delta v(t_1) + \delta_1 [\dot{s}(t_1) - \dot{v}(t_1)]. \end{aligned} \tag{A.14}$$

Thus the perturbation in the firing time δ_1 is approximately given by

$$\delta_1 \approx \frac{\delta s(t_1) - \delta v(t_1)}{\dot{v}(t_1) - \dot{s}(t_1)}, \tag{A.15}$$

where we have assumed that the denominator is not zero. At $t = (t_1 + \delta_1)^+$, we have:

$$\begin{aligned} \delta s[(t_1 + \delta_1)^+] &= s_p[(t_1 + \delta_1)^+] - s[(t_1 + \delta_1)^+] \approx s_0 + W[s_p(t_1) + \delta_1 \dot{s}_p(t_1), \alpha] - s(t_1^+) - \delta_1 \dot{s}(t_1^+) \\ &\approx s_0 + W[s_p(t_1), \alpha] + \delta_1 \dot{s}_p(t_1) W'[s_p(t_1), \alpha] - s(t_1^+) - \delta_1 \dot{s}(t_1^+) \\ &\approx \delta s(t_1) W'[s(t_1), \alpha] + \delta_1 \{\dot{s}(t_1) W'[s(t_1), \alpha] - \dot{s}(t_1^+)\}, \end{aligned} \tag{A.16}$$

where $W'[s, \alpha] \equiv \partial W / \partial s[s, \alpha]$. Furthermore, we have:

$$\delta v[(t_1 + \delta_1)^+] = v_p[(t_1 + \delta_1)^+] - v[(t_1 + \delta_1)^+] \approx -\delta_1 \dot{v}(t_1^+). \tag{A.17}$$

Using Eqs. (A.15)–(A.17), we get that:

$$\delta v[(t_1 + \delta_1)^+] = \alpha_{t_1} \delta v(t_1) - \alpha_{t_1} \delta s(t_1), \tag{A.18}$$

$$\delta s[(t_1 + \delta_1)^+] = -\beta_{t_1} \delta v(t_1) + (\beta_{t_1} + \gamma_{t_1}) \delta s(t_1) \tag{A.19}$$

with α_{t_1}, β_{t_1}, γ_{t_1} given in Eqs. (A.4)–(A.6). This finishes the computation of A_{t_1}.

A.2. Lyapunov exponent of the reduced model

The reduced model has only one dynamical variable, namely the threshold. The evolution of small threshold perturbations $\delta\hat{s}$ at successive discharge times is given by

$$\delta\hat{s}(t_{n+1}) = d_n \delta\hat{s}(t_n), \tag{A.20}$$

where a calculation similar to the one in Section 3 yields:

$$d_n = \left\{ W'[\hat{v}(t_n), \alpha] + \frac{W'[\hat{v}(t_n), \alpha]\{s_r - \hat{v}(t_n)\} + s_0 - s_r + W[\hat{v}(t_n), \alpha]}{\tau_s \dot{\hat{v}}(t_n) + \hat{v}(t_n)} \right\} \mathrm{e}^{-\Delta_{n+1}}. \tag{A.21}$$

Finally, the Lyapunov exponent of the reduced model can be defined as

$$\Gamma_{\mathrm{map}} = \lim_{n\to\infty} \frac{1}{t_n - t_1} \sum_{i=1}^{n} \ln |d_n|. \tag{A.22}$$

This equation was used in the numerical results.

References

[1] K. Aihara, G. Matsumoto, Y. Ikegaya, Periodic and non-periodic responses of a periodically forced Hodgkin–Huxley oscillator, J. Theor. Biol. 109 (1984) 249–269.
[2] P. Alström, B. Christiansen, M.T. Levinsen, Nonchaotic transition from quasiperiodicity to complete phase locking, Phys. Rev. Lett. 61 (1988) 1679–1682.
[3] C. Ascoli, M. Barbi, S. Chillemi, D. Petracchi, Phase-locked responses in the limulus lateral eye. Theoretical and experimental investigation, Biophys. J. 19 (1977) 219–240.
[4] R. Azouz, C.M. Gray, Cellular mechanisms contributing to the response variability of cortical neurons in vivo, J. Neurosci. 19 (1999) 2209–2223.
[5] E.A. Blair, J. Erlanger, On the process of excitation by brief electric shocks in axons, Am. J. Phys. 114 (1935/1936) 309–316.
[6] P.L. Boyland, Bifurcations of circle maps: Arnold tongues, bistability and rotation intervals, Commun. Math. Phys. 106 (1986) 353–381.
[7] M.J. Chacron, A. Longtin, M. St-Hilaire, L. Maler, Suprathreshold stochastic firing dynamics with memory in P-type electroreceptors, Phys. Rev. Lett. 85 (2000) 1576–1579.
[8] M.J. Chacron, A. Longtin, L. Maler, Negative interspike interval correlations increase the neuronal capacity for encoding time dependent stimuli, J. Neurosci. 21 (2001) 5328–5343.
[9] M.J. Chacron, K. Pakdaman, A. Longtin, Interspike interval correlations, memory, adaptation, and refractoriness in a leaky integrate-and-fire model with threshold fatigue, Neural Comp. 15 (2003) 253–278.
[10] S. Coombes, Liapunov exponents and mode-locked solutions for integrate-and-fire dynamical systems, Phys. Lett. A 255 (1999) 49–57.
[11] B. Ermentrout, M. Pascal, B. Gutkin, The effects of spike frequency adaptation and negative feedback on the synchronization of neural oscillators, Neural Comp. 13 (2001) 1285–1310.
[12] A.S. French, A.V. Holden, R.B. Stein, The estimation of the frequency response function of a mechanoreceptor, Kybernetika 11 (1972) 15–23.
[13] C.D. Geisler, J.M. Goldberg, A stochastic model of the repetitive activity of neurons, Biophys. J. 7 (1966) 53–69.
[14] L. Glass, M.C. Mackey, A simple model for phase locking of biological oscillators, J. Math. Biol. 7 (4) (1979) 339–352.
[15] M.S. Goldman, P. Maldonado, L.F. Abbott, Redundancy reduction and sustained firing with stochastic depressing synapses, J. Neurosci. 22 (2002) 584–591.
[16] H. Hayashi, S. Ishizuka, M. Ohta, K. Hirakawa, Chaotic behavior in the Onchidium giant neuron under sinusoidal forcing, Phys. Lett. A 88 (1982) 435–438.
[17] D. Horn, M. Usher, Neural networks with dynamical thresholds, Phys. Rev. A 40 (1989) 1036–1044.
[18] J. Keat, P. Reinagel, R.C. Reid, M. Meister, Predicting every spike: a model for the response of visual neurons, Neuron 30 (2001) 803–817.
[19] J.P. Keener, F.C. Hoppensteadt, J. Rinzel, Integrate-and-fire models of nerve membrane response to oscillatory input, SIAM J. Appl. Math. 41 (1981) 503–517.
[20] B.W. Knight, Dynamics of encoding in a population of neurons, J. Gen. Physiol. 59 (1972) 734–766.
[21] M. Kunze, Non-smooth dynamical systems, in: Lecture Notes in Mathematics, Springer-Verlag, Berlin, 2000.

[22] P. Le Calvez, Dynamical properties of diffeomorphisms of the annulus and of the torus, in: American Mathematical Society, Providence, RI, Société Mathématiques de France, Paris, 2000.
[23] Y.H. Liu, X.J. Wang, Spike frequency adaptation of a generalized leaky integrate-and-fire neuron, J. Comput. Neurosci. 10 (2001) 25–45.
[24] A. Longtin, C. Laing, M.J. Chacron, Correlations and memory in neurodynamical systems, in: G. Rangarajan, M. Ding (Eds.), Long-range Dependent Stochastic Processes: Theory and Applications, Springer, Berlin, 2003.
[25] P.C. Muller, Calculation of Lyapunov exponents for dynamical systems with discontinuities, Solitons Fract. 5 (1995) 1671–1681.
[26] K. Pakdaman, Periodically forced leaky integrate-and-fire model, Phys. Rev. E 63 (2001) 041907.
[27] K. Pakdaman, J.F. Vibert, Modeling excitatory networks, J. Sci. 34 (1995) 788–793.
[28] K. Pakdaman, J.F. Vibert, E. Boussard, N. Azmy, Single neuron with recurrent excitation: effect of the transmission delay, Neural Networks 9 (1996) 797–818.
[29] J.W.S. Pringle, V.J. Wilson, The response of a sense organ to a harmonic stimulus, J. Exp. Biol. 29 (1952) 220–235.
[30] A. Rescigno, R.B. Stein, R.L. Purple, R.E. Poppele, A neuronal model for the discharge patterns produced by cyclic inputs, Bull. Math. Biophys. 32 (1970) 337–353.
[31] D. Ruelle, Chaotic Evolution and Strange Attractors: The Statistical Analysis of Time Series for Deterministic Nonlinear Systems, Cambridge University Press, Cambridge, 1989.
[32] J.P. Segundo, D.H. Perkel, H. Wyman, H. Hegstad, G.P. Moore, Input output relations in computer simulated nerve cells, Kybernetika 4 (1968) 157–175.
[33] R.B. Stein, A.S. French, A.V. Holden, The frequency response, coherence, and information capacity of two neuronal models, Biophys. J. 12 (1972) 295–322.
[34] H.C. Tuckwell, Introduction to Theoretical Neurobiology: I. Cambridge University Press, Cambridge, 1988.
[35] J.F. Vibert, K. Pakdaman, N. Azmy, Inter-neural delay modification synchronizes biologically plausible neural networks, Neural Networks 7 (1994) 589–607.
[36] J.F. Vibert, J.P. Segundo, Slowly adapting stretch-receptor organs: periodic stimulation with and without perturbations, Biol. Cybern. 33 (1979) 81–95.